PAPER

Check for updates

The density, nanohardness and some optical properties of As–S and As–Se chalcogenide bulk glasses and thin films†

P. Knotek, [ID] b P. Kutálek, [ID] *a E. Černošková, [ID] a M. Vlček a and L. Tichý [ID] b

Amorphous As_2S_3, As_2Se_3 and As_1Se_{99} bulk glasses and thin films were prepared by the melt quenching technique and vacuum thermal evaporation, respectively, on different substrates. The density (ρ) – determined by the simple and cheap method of precise weighting, refractive index (n), structural arrangement – inferred from Raman spectroscopy, and nanohardness (H_{ind}) were determined for all the studied materials in both bulk and thin film states. It is found that regardless of the chemical composition, the bulk glass density, refractive index and nanohardness are higher in comparison with those of the corresponding virgin and by annealing relaxed thin films, and the observed differences are discussed. The almost negligible influence of the substrate on the thin films density, structural arrangement and nanohardness, was observed.

1. Introduction

Chalcogenide glasses and amorphous thin films possess some interesting properties such as a non-linear optical properties, high infrared transparency, high refractive index, photosensitivity *etc.* Therefore, they remain a key subject of study and find utilization in many promising applications such as an infrared technology, integrated and nonlinear optics, phase change memory, *etc.*[1,2] Also the structural arrangement of chalcogenide glasses is still of interest.[3–5]

One of the important mechanical characteristics of solids is density, which affects various optical, electrical and mechanical properties. Changes in density can significantly influence the refractive index of a material as it follows for example, from the Lorentz–Lorenz relation.[6,7] For optical memories, that use inclusive phase change materials (PCM), the density changes indicate the possibility to reach a high optical contrast. On the contrary, the absence of density changes is preferred in the case of phase change random access memories (PCRAM), where density changes could lead to failure of a device due to stress between, for example, electrodes and PCM layers.[8] In many amorphous chalcogenides the intrinsic photodarkening is associated with a change in the sample thickness, it means density changes, which reflect some photo induced structural

changes in the material.[9,10] Although the density of many materials in the bulk form is well known and easy to determine, this is not always the case for materials in a thin film form.

Some ways to determine thin film density have been reported in the literature. For example, the density of metallic films was obtained by Samuelsson *et al.* employing Rutherford backscattering spectrometry.[11] Waseda *et al.*[12] described the determination of molybdenum thin film density using a pressure-of-flotation method. The determination of the thin film density of amorphous germanium measured by an *in situ* and non-destructive method based on a quartz single-crystal oscillator, was described by Viščor *et al.*[13] Another important non-destructive method is X-ray reflectivity measurement.[14] For some other different approaches, including the Swanepoel method, see for example ref. 15–18.

The other mechanical property which is important not only for thin film applications, but also for improved understanding of the structure and other physical and chemical properties of thin films, is the nanoindentation hardness (nanohardness), developed as a depth-sensing indentation technique in 1983.[19,20] The nanohardness of chalcogenide bulk glass and thin films are not frequently studied or even compared. Ge–Se chalcogenide bulk glasses were, for example, studied by Guin *et al.*[21] from the point of hardness, toughness and scratchability. They discussed the hardness and fracture toughness as the result of structural models accounting for the topological changes occurring in a glass network. As_2Se_3 thin films with combined nanoindentation and AFM methods by Trunov *et al.*[22] were investigated, and the authors used the multi-cycling test to probe the local photomechanical response of the thin films. Also Sabapathy *et al.*[23] and Ding *et al.*[24] studied nanoindentation in waveguides and thin films, respectively. The mechanical

aUniversity of Pardubice, Faculty of Chemical Technology, Joint Laboratory of Solid State Chemistry, Studentská 84, 532 10 Pardubice, Czech Republic. E-mail: petr.kutalek@upce.cz; Tel: +420 466036155

bUniversity of Pardubice, Faculty of Chemical Technology, Department of General and Inorganic Chemistry, Studentská 573, 532 10 Pardubice, Czech Republic

† Electronic supplementary information (ESI) available. See DOI: 10.1039/d0ra08939g

properties of chalcogenide glasses by Rajakumar *et al.*[25] and Prabhudessai *et al.*[26] were studied, however, from the point of Vicker's hardness.

In the present paper, we studied namely the density and nanohardness of virgin and relaxed (annealed) amorphous chalcogenide thin films. To determine the density of studied thin films we used the method of precise weighting. This method is suitable for the single layer thin films with a thickness of around 1 μm and higher, it is simple and does not require expensive and sophisticated equipment. For the comparative reasons we used canonical glasses As_2S_3, As_2Se_3 and As_1Se_{99} and we characterized the bulk glasses and thin films using UV-Vis spectroscopy, Raman scattering, differential scanning calorimetry and nanoindentation.

2. Experimental

2.1. Sample preparation

The As_2S_3, As_2Se_3 and As_1Se_{99} bulk glasses were prepared using the classical melt-quenching technique from stoichiometric amounts of pure (5 N) elements. For more experimental details, see ref. 27. After quenching in air, the ampoules were annealed at around $T_g - 50$ °C, where T_g is the glass transition temperature of the corresponding bulk glass, for approximately 4 h. The amorphous films were made by means of vacuum thermal evaporation TE (Balzers BAE 250T coating system, $p \approx 10^{-3}$ Pa, rate of evaporation 2–2.5 nm s^{-1}, the substrates rotation rate ≈ 15 rpm) from the previously synthesized bulk glasses onto microscope glass and Si substrates. The chemical composition of the prepared bulk glasses and thin films was checked using electron microprobe X-ray analysis (Jeol JSM5500 LV equipped with GRESHAM Sirius 10 detector), the estimated error in the determination of chemical composition was ±1 at% for thin films and ±0.5 at% for bulk glasses. The amorphous state of all bulk glasses and corresponding thin films with XRD analysis was proven (see Fig. A. 1A and B, respectively).†

2.2. Sample characterization

For comparative reasons, the virgin (vir.), annealed relaxed thin films (ann.) and bulk glasses (bulk; polished to optical quality) were characterized by the following methods:

(i) Using UV-Vis spectroscopy in the region of the short wavelength absorption edge (SWAE) and in the transparent region employing a PerkinElmer Lambda 12 spectrophotometer (the spectral region 330–1100 nm). A modified Swanepoel method[18] was used for the determination of the refractive index (n) and the thickness (d) of virgin and annealed thin films (4 h, (T_g(bulk) × 0.9–50) °C) from the optical transmission spectra. The thickness of thin films employing a scanning electron microscope (SEM, Jeol JSM5500 LV) on the freshly broken films was also checked. The refractive index (n) of bulk glasses was calculated according to the formula $n = 1/T_0 + (1/T_0^2 - 1)^{1/2}$, where T_0 is the transmittance in the transparent region (at wavelength 1000 nm) of the bulk glass. The optical band gap values (E_g^{opt}) of the thin films according to the Tauc model[28] were determined.

(ii) Raman spectra were measured with a confocal Raman microscope LabRam HR (Horiba Jobin Yvon) using a 785 nm excitation, magnification 10× and 20 mW intensity. The intensity by the photodiode sensor coupled to Nova Handheld Laser Power Meter (Ophir, Israel) at the exit of the microscope was measured. The total number of scans was 10 with a 5 s exposition for each spectrum. In addition, the intensities of the bands in the Raman spectra using Gammon–Shuker formula[29] were reduced and normalized to the most intensive band.

(iii) The bulk glasses were characterized by differential scanning calorimetry (DSC, Diamond PerkinElmer); 10 mg of the powdered samples in sealed alumina pans was used, the heating rate was set to 10 °C min^{-1}.

2.3. Density and nanohardness measurements

(i) The Archimedean density (ρ_{bulk}) of the glasses with bulk samples was measured in ethylene glycol. Using ten measurements, the determination standard error of density at around ±0.0005 g cm^{-3} was estimated.

The determination of thin films density (ρ_{film}) requires several steps and it was calculated as $\rho_{film} = (m_{sub+film} - m_{sub})/(S \times d)$, where $m_{sub+film}$ and m_{sub} are the weight of substrate with and without the thin film in grams, respectively, S is the area of evaporated thin film onto the substrate in cm^2, and d is the thickness of the prepared thin films in cm. In the first step, it was necessary to determine the precise weight of the thin films (the difference between the $m_{sub+film}$ and m_{sub}) evaporated onto substrates. For this purpose, the very accurate UMX balance (Mettler Toledo) with readability 0.1 μg was used. For comparison, we also used the RESEARCH (SARTORIUS) balance with lower readability (10 μg) in comparison with the UMX balance. The readability and repeatability of both balances was tested by weighting of the same clean glass substrate for 10 times and the results are displayed in the form of a box-plot in Fig. A. 2.† After weighting the clean substrates 10 times (m_{sub}), the thin films were evaporated onto them and the weight of thin film plus substrate was determined ($m_{sub+film}$), and the weight of the thin film was calculated. The thickness (d) of each prepared thin film evaporated onto glass substrate by modified Swanepoel method and SEM analysis was determined, and the mean from 8 values was used for the calculation of thin film density. It also should be noted that we assume the uniform and homogenous thickness of all thin films on different substrates, which was achieved by their rotation during the evaporation. We also excluded the presence of thin films with a wedge-shape which may lead to errors in the determination of refractive index and thickness values as described by Márquez *et al.*,[30] by taking several measurements at different places of the same substrate. The area of evaporated thin films on different substrates (S) was determined from the relevant optical images using a simple version of an automatic threshold detection technique.[31–33] For example, the area of the As_2S_3 thin film evaporated onto glass substrate equals 4.54$_9$ cm^2 with the standard deviation 0.002 cm^2 from five independent evaluations. The area of other thin films evaporated on different substrates in the same way was
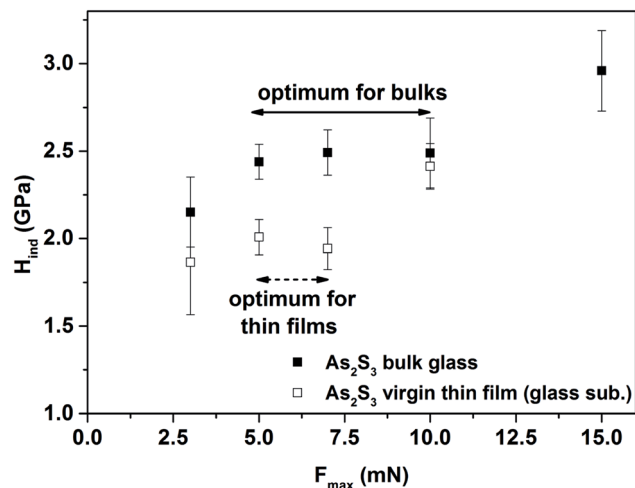
Fig. 1 The dependency of nanohardness (H_{ind}) on a different peak load (F_{max}) for As₂S₃ bulk glass and virgin thin film evaporated onto a glass substrate.

determined. Furthermore, the standard deviations in the area of evaporated thin films did not exceed 0.05% in all cases.

(ii) The nanoindentation measurements were done for the bulk glasses and corresponding thin films evaporated onto different substrates (glass and Si), employing an atomic force microscope (AFM, SOLVER NEXT, NT-MDT) equipped with a nanoindentation head NS01NTF and a Berkovich type of tip (trigonal pyramid geometry with a parameter of static stiffness, $k = (10.2 \pm 0.3)$ kN m^{-1}). Fused silica SiO₂ was used as a calibration sample (hardness, $H = (9.5 \pm 0.5)$ GPa by ISO 9450-76). The penetration depth of the tip was up to a maximum 10% of the total thickness of thin films. The distance between individual indentation points was more than two times the diagonal length in order to avoid any mutual interference of indentations. A peak load, F_{max}, was varied between 3–15 mN, while the optimum for the comparison of bulk glasses and corresponding thin films was found at $F_{max} = 5$ mN and hence all samples at this value were compared (see Fig. 1). Post-indentation, the images of the imprints immediately were captured. A minimum of 9 indentations were performed for each sample/treatment. The F–h (force-displacement) curves were analyzed using the Oliver–Pharr method[34] to extract the nanoindentation hardness

(H_{ind}) of the glasses and thin films. The standard error in the determination of H did not exceed 0.08 GPa in any case.

3. Results and discussion

3.1. Chemical composition and characteristics of the studied materials

The results of chemical composition analysis for all the prepared thin films in Table 1 are summarized. It is clear that for the bulk glasses the nominal chemical composition corresponds well with the results of the electron microprobe X-ray analysis. It also could be seen that the chemical composition of all prepared thin films was, with respect to the experimental error, comparable to that of the corresponding bulk glasses. Additionally, in the whole manuscript the samples are marked as As₂S₃ for As₄₀S₆₀ bulk glass and As₃₉.₀S₆₁.₀ thin film (both in atomic fractions); As₂Se₃ for As₄₀Se₆₀ bulk glass and As₄₁.₂S₅₈.₈ thin film (both in atomic fractions); and as As₁Se₉₉ for As₁Se₉₉ bulk glass and As₀.₅S₉₉.₅ thin film (both in atomic fractions). The glass transition temperatures, see Table 1, (determined as the mid-point by DSC) for the bulk glasses, correspond well to those reported in the literature.[35,36] The effect of the so-called "useful impurity" for the As₁Se₉₉ bulk glass[1,37] that causes an increase in the glass transition temperature even by the addition of 1 at% of As into pure amorphous Se (due to the cross-linking of the selenium matrix by arsenic atoms) is evident (for the T_g values[38]). Table 1 also shows the basic optical characteristics (the optical band gap (E_g^{opt}) and refractive index (n)) for all prepared thin films evaporated onto a glass substrate. The optical band gap of As₂S₃ virgin thin film evaporated onto glass substrate is 2.38 eV while for As₂Se₃ and As₁Se₉₉ it decreases to 1.78 and 1.89 eV, respectively. The values of the optical band gap E_g^{opt} correspond well to those reported in the literature.[10,39]

Finally, Table 1 also summarizes the values of all thin film thicknesses determined by the modified Swanepoel method.[18] It should be noted that these are average values of the thin film thickness measured from 8 different places on the substrate. The typical conformity between the experimental and fit of experimental data is shown in Fig. 2A for the As₂S₃ thin film evaporated onto a glass substrate. It could be seen that the thickness of all thin films evaporated onto the glass substrate is in the range 3–4 μm. It also should be noted that the standard

Table 1 The experimental chemical composition for all prepared bulk glasses and virgin thin films, the bulk glass transition temperature (mid-point) and refractive index and the basic optical parameter of all virgin thin films

	Bulk glasses			Thin films			
Sample	Chemical composition (at%) As : X, where X = S, Se	T_g (°C)	Refractive index (—)	Chemical composition (at%) As : X, where X = S, Se	Refractive index (—)	E_g^{opt} (eV)	d (nm)
As₂S₃	40 : 60	205	2.42	39.0 : 61.0	2.40, 2.41^a	2.38	3370
As₂Se₃	40 : 60	190	2.84	41.2 : 58.8	2.69	1.78	3260
As₁Se₉₉	1 : 99	55	2.52	0.5 : 99.5	2.49	1.89	3910

^{a} The refractive index of As₂S₃ thin film evaporated onto glass substrate after the annealing.
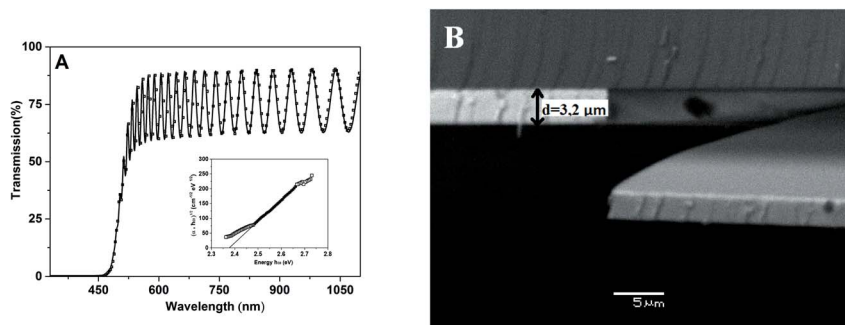
Fig. 2 The experimental (solid line) and fit of calculated values (symbols) of spectral dependency of the optical transmission for the As_2S_3 virgin thin film evaporated onto a glass substrate (A), and SEM image of fresh As_2S_3 virgin thin film broken perpendicularly to the direction of evaporation (B). The inset in (A) shows the spectral dependency of the absorption coefficient for the As_2S_3 virgin thin film evaporated onto the glass substrate.

deviation in the determination of all thin film thicknesses by the modified Swanepoel method do not exceed 0.5%. The thickness of all thin films was also checked by SEM analysis on fresh samples broken perpendicularly to the direction of evaporation, and the comparable results, with respect to the 2% experimental error, were obtained as is shown for the As_2S_3 thin film evaporated onto the glass substrate in Fig. 2B.

3.2. Raman spectra of the bulk glasses and thin films

Fig. 3A gives the Raman spectra of As_2S_3 bulk glass and thin films evaporated onto glass and Si substrates, and as is well

known, the spectra of the thin films are different to the spectra of bulk glass. The spectra of bulk glass consists of the main broad band with the maxima at ≈ 340 cm^{-1} corresponding to the presence of symmetric stretching vibration modes of $AsS_{3/2}$ pyramidal units with two shoulders at ≈ 310 and 380 cm^{-1} attributed to the presence of the antisymmetric stretching vibration modes of $AsS_{3/2}$ pyramidal units and As–S–As bridges, respectively. The weak bands near ≈ 190 and 230 cm^{-1} are attributed to the presence of the bending vibration mode of As–As molecular units. In contrast, the bands at ≈ 340 and 360 cm^{-1} dominate the spectra of As_2S_3 thin films evaporated

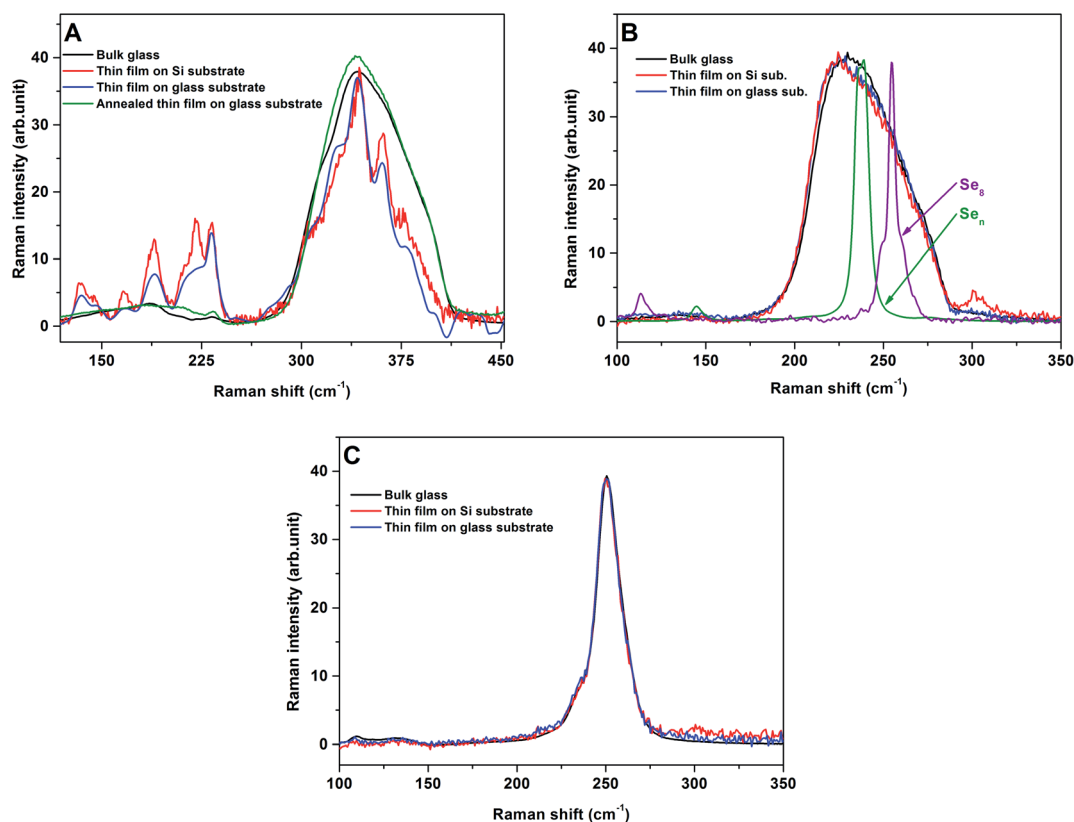**Fig. 3** Raman spectra of As_2S_3 (A), As_2Se_3 (B) and As_1Se_{99} (C) bulk glasses and thin films (virgin/annealed) evaporated onto glass and Si substrates. For comparison reasons, also included in (B) is the Raman spectra of pure glassy Se consisting mainly of Se_8 rings or Se_n chains according to ref. 62.

onto glass and Si substrates, and they have been assigned to the symmetric and antisymmetric stretching vibration modes of As–S bond in β-As_4S_4 molecular units, respectively. The bands at ≈190 and 220 cm^{-1} in the bending vibration region have been attributed to the S–As–S bending mode in the As_4S_4 molecular units, and the band at ≈230 cm^{-1} has been associated with the bending of $S_2As–AsS_2$ structural units. The bands at ≈145 and 165 cm^{-1} correspond to the vibration in As_4S_4 molecular units, while the band at ≈134 cm^{-1} is connected to the presence of $AsS_{3/2}$ pyramidal units.[40–45] After the annealing, the Raman spectra of the As_2S_3 thin film evaporated onto glass substrate becomes comparable to that of bulk glass (Fig. 3A). Similar results are published in ref. 9, 46 and 47 and are explained by the temperature induced bond rearrangement and a network polymerization.

Contrary to As_2S_3 bulk glass and thin films, the Raman spectra of As_2Se_3 bulk glass and thin films evaporated onto glass and Si substrates are practically identical (Fig. 3B). The Raman spectra of all the samples consist of a broad band between 200–300 cm^{-1} which is formed by overlapping the main band near 220–230 cm^{-1} connected with the stretching vibration modes of $AsSe_{3/2}$ pyramidal units, the band near 235 cm^{-1} is attributed to the presence of –(Se–Se)$_n$– ($n \geq 1$) chain vibrations, and the band near 255 cm^{-1} is assigned to the presence of both Se_8 rings and Se_8 meandering chain vibrations.[48] A comparable result for the Raman spectra of As_1Se_{99} bulk glass and the corresponding thin films evaporated onto glass and Si substrates was also found, as shown Fig. 3C. In this case, the Raman spectra of all samples consist only of one main band over 250 cm^{-1} which is formed by the overlapping of the most intense band at 255 cm^{-1} and the band near 235 cm^{-1} and they were attributed as described above. Hence, the Raman spectra of all studied bulk glasses and thin films well corresponds to the literature data[9,46–48] and practically no influence on the substrates was observed on the Raman spectra of the prepared thin films.

3.3. Density of the bulk glasses and thin films

Table 2 summarizes the Archimedean bulk glasses density (ρ_{bulk}) and the density of the corresponding thin films (ρ_{film}) evaporated onto different substrates. The bulk density varied

from 3.193$_8$ g cm^{-3} for As_2S_3 bulk glass to 4.55$_7$ and 4.295$_7$ g cm^{-3} for As_2Se_3 and As_1Se_{99} bulk glasses, respectively. Comparable trends for the density of bulk glasses and the density of corresponding thin films, were found. The density varied from 3.14$_7$ g cm^{-3} for the As_2S_3 thin film evaporated onto the glass substrate, to 4.22$_7$ and 4.19$_8$ g cm^{-3} for As_2Se_3 and As_1Se_{99} thin films evaporated onto the same substrate, respectively. These values are comparable to those reported in the literature.[36,49] The density for thin films evaporated onto Si substrate varied from 3.14$_8$ g cm^{-3} for As_2S_3 to 4.23$_7$ and 4.21$_6$ g cm^{-3} for As_2Se_3 and As_1Se_{99}, respectively. Thus almost negligible influence of substrate at the given films thickness (see Table 1) on the thin films density was observed (Table 2). The decrease of thin films density in comparison with the corresponding bulk glass equals ≈2 rel% for As_2S_3 and As_1Se_{99}, and to ≈8 rel% for As_2Se_3 materials (Table 2). Hence, it is seen that regardless of the chemical composition and also the used substrates for the preparation of thin films, the bulk glasses density (ρ_{bulk}) is higher than the density of the corresponding thin films (ρ_{film}). It also should be mentioned that the cumulative error (uncertainty) of the thin films density values, calculated according to ref. 50, do not exceed 0.5% in all cases (it varies from ≈0.016 to ≈0.021 g cm^{-3} based on the chemical composition and the substrate used for the evaporation). The comparable trend, as shown in this work, was also published by De Neufville *et al.*[51] for the As_2Se_3 bulk glass and corresponding evaporated thin film. However, the authors also compared the density of As_2S_3 bulk glass and corresponding thin film and in this case, the density variation was opposite which was not commented by the authors. Table 2 additionally shows that the density of the As_2S_3 thin film increased to 3.16$_0$ g cm^{-3} after the annealing of this thin film.

3.4. Refractive index

The refractive indices (n) for all the prepared bulk glasses and corresponding virgin thin films evaporated onto the glass substrates are shown in Table 1. The comparable values of the bulk glass refractive index, for example by Cardinal *et al.*,[36] have been published. From Table 1 it is clear that: (i) regardless of the chemical composition, the refractive index of the thin films is lower than the refractive index of the corresponding bulk glasses, and (ii) the refractive index decrease is equal to ≈1 rel% for As_2S_3 and As_1Se_{99} thin films, and ≈5 rel% for the As_2Se_3 thin film, in comparison with the corresponding bulk glasses. De Neufville *et al.*[51] also show in their work that As_2S_3 bulk glass has a higher refractive index than the corresponding virgin thin film. The authors also found much higher difference in the refractive index than that reported in this work which, however, could be a consequence of different preparation conditions. Furthermore, the authors showed that the refractive index of virgin As_2S_3 thin film after annealing and illumination is almost the same as that of bulk glass. Additionally, Table 1 also shows that after annealing of the As_2S_3 virgin thin film evaporated onto glass substrate, the refractive index increased to the value of 2.41.

Table 2 The density of all bulk glasses and corresponding virgin thin films evaporated onto different substrates

Sample	ρ_{bulk}^{a} (g cm^{-3})	$\rho_{thin\ film}$ on different substrates^{a} (g cm^{-3})		$\rho_{bulk}/\varnothing\ \rho_{thin\ films}^{a}$
		Glass	Si	
As_2S_3	3.193$_8$	3.14$_7$; 3.16$_0^{b}$	3.14$_8$	1.01$_5$/1.01$_1^{b}$
As_2Se_3	4.558$_7$	4.22$_7$	4.23$_7$	1.07$_7$
As_1Se_{99}	4.295$_7$	4.19$_8$	4.21$_6$	1.02$_1$

^{a} The number in the subscript expresses the highest value of uncertainty found in a similar manner to that one used previous in ref. 63. ^{b} The density (or $\rho_{bulk}/\varnothing\ \rho_{thin\ film}$ ratio) for As_2S_3 thin film evaporated onto glass substrate after the annealing.

We shall try to compare the changes in the refractive index and density of the bulk samples and virgin films employing the Lorentz–Lorenz relation (LLR): $(n^2 - 1)/(n^2 + 2) = \rho R_m$, $R_m = 4\pi N_A \alpha_m/3$, where α_m is the molecule polarizability and N_A is the Avogadro number. Because we did not observe the dimension changes in the direction parallel to the substrate, we assume that the volume (V) changes of the film correspond mainly to the expansion, that is to an increase in the film thickness (d). In such a case: $\Delta d/d = \Delta V/V = -\Delta\rho/\rho$, (we assume: $dx/x = \Delta x/x$; where $\Delta X = X_{ann.} - X_{vir.}$ or $\Delta X = X_{bulk} - X_{vir.}$). Hence from LLR follows: $\Delta n_{(LL)} = [(\Delta\rho/\rho) + (\Delta R_m/R_m)](n^2 - 1)(n^2 + 2)/6n$, assuming that $\Delta R_m/R_m \neq 0$. For the experimental values of refractive indices and densities of virgin films and bulk glasses, see Table 1, we obtain $\Delta n_{(exp)} = \Delta n_{(LLR)}$ only assuming that $\Delta R_m/R_m = -0.007, -0.036$ and -0.012 for As_2S_3, As_2Se_3 and As_1Se_{99}, respectively. This means that in the considered cases the differences in the densities cannot be fully explained by the differences between refractive indices of the bulks and virgin thin films. However, with respect to the magnitude of $\Delta R_m/R_m$ the values of $\Delta\rho/\rho$ play a major role in the observed $\Delta n_{(exp)}$ differences ($\Delta\rho/\rho = 0.0149, 0.0785$ and 0.0233 for As_2S_3, As_2Se_3 and As_1Se_{99}, respectively). This finding is interesting with respect to the results of Raman spectroscopy as the structural differences between bulk and virgin thin film of As_2Se_3 and As_1Se_{99} are very small in comparison with those of As_2S_3 (comparing Fig. 3A–C). We note that for As_2Se_3 quite small structural differences inferred from Raman spectroscopy between the bulk and virgin thin film in the work by Němec et al.[10] and Treacy et al.[52] were also found. For large structural differences for As_2S_3, see Fig. 3A, we observed the lowest change in $\Delta\rho/\rho$. This we tentatively explain by assuming that a density decrease of As_2S_3 virgin thin film, associated with the depolymerization of the network and with an increase in disorder, is compensated by As_4S_4 structural units present in the virgin thin film having higher density ($\rho_{realgar} = 3.56$ g cm^{-3}/$\rho_{pararealgar} = 3.52$ g cm^{-3} (ref. 53)) than As_2S_3 bulk. Of interest is the fact that contrary to the As_2S_3 case, for both As_1Se_{99} and As_2Se_3, there are only very subtle structural differences indicated by Raman spectroscopy, see Fig. 3B and C, while there are evident and higher differences in the density in comparison with the As_2S_3 case. We suppose that this finding could be qualitatively explained assuming that the major part of the observed density difference is attributed to higher empty volume in virgin As_1Se_{99} and As_2Se_3 thin films. Hence the difference in the refractive index of As_1Se_{99} and As_2Se_3 thin films and bulk, and the corresponding virgin thin films, is not associated with the large structural changes, but rather it can be attributed to a reduction of empty volume[1] in the bulk samples, and of course to the changes in molar polarizability. Since $\Delta R = \alpha_{m,bulk} - \alpha_{m,vir.}$, the negative values of ΔR (see previous text) mean that $\alpha_{m,vir.} > \alpha_{m,bulk}$. Consequently one can speculate that higher disorder associated with the presence of wrong bonds, defect states, possible fluctuation in the bond length and bond distances can assist an increase of molar polarizability of As_1Se_{99} and As_2Se_3 virgin thin films.

For similar comparison of the virgin and annealed states of the As_2S_3 thin film (the data in Tables 1 and 2), we can obtain

$\Delta n_{(LL)} = 0.01$ which is comparable to the experimental value, even for $\Delta R_m/R_m = 0$. This means, with respect to the experimental error, that $R_{m,vir.} = R_{m,ann.}$ and hence $\alpha_{m,vir.} = \alpha_{m,ann.}$. This behavior needs further attention and will be the subject of further research.

3.5. The nanoindentation hardness of bulk glasses and thin films

Fig. 4 shows the representative force (F)–displacement (h) curve for the As_2Se_3 thin film evaporated onto a glass substrate, and the subtracted values of maximal displacement (h_{max}) at the set peak load (F_{max}), and the slope of unloading curve ($S_{BW} = dF/dh$). For all the bulk glasses and thin films evaporated onto different substrates, smooth F–h curves with residual depth upon complete unloading were observed. The homogeneous deformation of material indicates the absence of pop-ins (or displacement bursts) in the loading part, while no pop-out or elbow during unloading reveals clearly that no phase transformation occurs (see Fig. 4). Furthermore, the inset of Fig. 4 shows the residual imprint image, with the shape of the trigonal pyramid created by the pushing of a Berkovich type of tip into the material, on the specimen surface captured immediately post-indentation. Fig. 4 also illustrates that during the indentation no corner cracking occurs. Table 3 summarizes the values of h_{max}, F_{max} and S_{BW} subtracted from the individual force–displacement curves for the As_2Se_3 thin film evaporated onto the glass substrate. The values of contact depth (h_c), using the Oliver–Pharr method (see eqn (3) in ref. 34), were calculated and based on the calibration, carried out on the fused silica reference sample, the values of A_c (the contact area) were determined. Finally, the Oliver–Pharr method was used (see eqn (5) in ref. 34) to extract the nanohardness (H_{ind}) of the As_2Se_3 thin film as shown in Table 3. It could be seen that from the nine independent indentations the average nanohardness (H_{ind}) of the As_2Se_3 thin film equals 1.88 GPa with standard deviation 0.05 GPa. The nanohardness (H_{ind}) of the rest of the bulk glasses
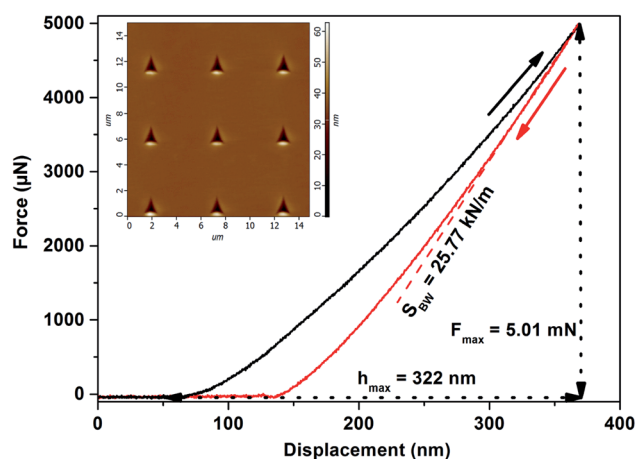

Fig. 4 The representative force (F)–displacement (h) curve for the As_2Se_3 virgin thin film evaporated onto glass substrate, and the subtracted values of h_{max}, F_{max} and S_{BW}. The inset shows the residual imprint on the specimen surface.

Table 3 The values of h_{max}, F_{max} and S_{BW} subtracted from the individual force–displacement curves, and the calculated values of h_c, A_c (according to the calibration), and H_{ind} using the Oliver–Pharr method for the As$_2$Se$_3$ virgin thin film evaporated onto the glass substrate. Also shown is the arithmetic mean of H_{ind} values (ar. mean) and its standard deviation (SD). A peak load $F_{max} = 5$ mN was used

N	h_{max} (nm)	F_{max} (mN)	S_{BW} (kN m^{-1})	h_c (nm)	A_c (µm^2)	H_{ind} (GPa)
1	322	4.96	26.45	181	2.70	1.8374
2	315	4.98	26.32	173	2.57	1.9353
3	325	4.97	24.87	175	2.60	1.9085
4	330	4.98	25.65	184	2.75	1.8137
5	326	4.98	25.15	177	2.64	1.8861
6	321	4.99	27.43	185	2.75	1.8156
7	320	4.98	25.69	175	2.60	1.9180
8	316	5.01	26.35	173	2.58	1.9434
9	322	5.01	25.77	176	2.62	1.9118
					Ar. mean	1.88
					SD	0.05

and the thin films on the different substrates was determined in the same way.

It also should be mentioned that the peak load, F_{max}, varied between 3–15 mN for all materials, while the optimum for the comparison of all bulk glasses and thin films evaporated onto different substrates was found at $F_{max} = 5$ mN (see Fig. 1), and hence the nanohardness of all the samples was compared at this value. If a higher F_{max} was used, the rule that the penetration depth of the tip was up to a maximum of 10% of the total thickness of the thin films, was not fulfilled, and the measured nanohardness could be influenced by the nanohardness of the substrate. On the other hand, for a lower F_{max}, the experimental error was higher than 20%, probably due to surface defects, experimental noise *etc.*

Table 4 summarizes the nanohardness (H_{ind}) of As$_2$S$_3$, As$_2$Se$_3$ and As$_1$Se$_{99}$ bulk glasses and the corresponding thin films evaporated onto different substrates. It could be seen that the almost comparable values of the H_{ind} for As$_2$S$_3$ and As$_2$Se$_3$ bulk glasses were observed. The comparable trend was also published by Kavetskyy *et al.*[54] However, the authors provided the values of microhardness for As$_2$S$_3$ and As$_2$Se$_3$ bulk glasses which were almost equal. The nanohardness, in our case, varied from 2.44 to 2.20 GPa for As$_2$S$_3$ and As$_2$Se$_3$ bulk glasses, respectively (Table 4). On the other hand, much lower

nanohardness of As$_1$Se$_{99}$ ($H_{ind} = 1.29$ GPa) in comparison with the As$_2$S$_3$ and As$_2$Se$_3$ bulk glasses was observed. This could be connected with its structure and it differs significantly in comparison with other prepared materials, see Fig. 3. In the case of As$_1$Se$_{99}$, mainly –(Se–Se)$_n$– ($n \geq 1$) chains and both Se$_8$ rings and Se$_8$ meandering chains were found.[48] The decrease of As$_1$Se$_{99}$ bulk glass nanohardness in comparison with As$_2$Se$_3$ bulk glass is in harmony with the results published by Guin *et al.*[21] The authors showed that Vicker's or Meyer's hardness increases with increasing average coordination number of Ge–Se chalcogenide bulk glasses and they supposed that the main reason for such behavior is the topological nature. Table 4 also compares the nanohardness of all the bulk glasses under the different peak load (F_{max}), while the trend in H_{ind} was not changed. This trend in nanohardness is in harmony with the data of microhardness published in the literature[55] for the same bulk glasses. We realize that this comparison of our results with that in the literature is not entirely correct, but to our best knowledge, there are no relevant data for nanohardness, for the glasses studied by us, for true comparison.

With some caution in comparing nanohardness and microhardness values, we show in Fig. 5, the empirical correlation H_{ind} and H_v values *versus* T_g values, where H_v and T_g values for Ch–As$_2$Ch$_3$ (Ch = S, Se) glasses were taken from ref. 55. It is

Table 4 The nanohardness (H_{ind}) of As$_2$S$_3$, As$_2$Se$_3$ and As$_1$Se$_{99}$ bulk glasses and their corresponding virgin thin films evaporated onto different substrates. The H_{ind} of all materials was compared at the same peak load ($F_{max} = 5$ mN). For comparison there are also the data of H_{ind} for all the bulk glasses for peak load ($F_{max} = 10$ mN), and the data for microhardness are taken from ref. 55

	Bulk glasses			Thin films nanohardness (GPa), ($F_{max} = 5$ mN)	
	Nanohardness (GPa)		Microhardness (kg mm^{-2})		
Sample	$F_{max} = 5$ mN	$F_{max} = 10$ mN	Data taken from ref. 55	Glass substrate	Si substrate
As$_2$S$_3$	2.44	2.49	1.33	2.01, 2.08^a	1.99
As$_2$Se$_3$	2.20	2.41	1.24	1.88	1.87
As$_1$Se$_{99}$	1.29	1.63	0.43	1.08	—

^{a} The nanohardness of As$_2$S$_3$ thin film evaporated onto a glass substrate after annealing.
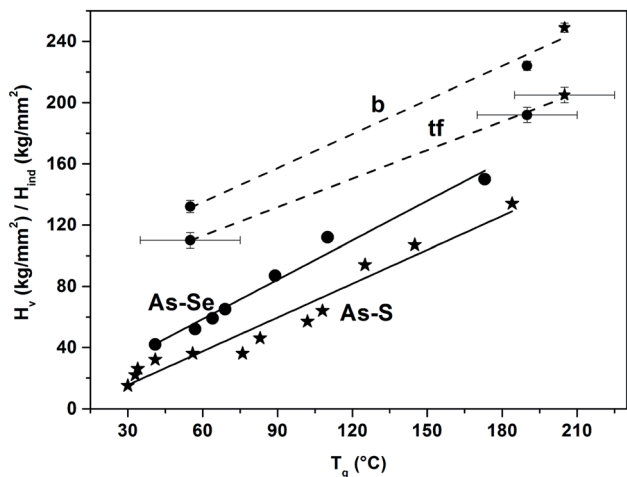
Fig. 5 The dependency of microhardness (H_v) on a glass transition temperature (T_g) for As–S (solid line with stars, $As_xS_{(100-x)}$, $9.1 \leq x \leq 40$) and As–Se (solid line with circles, $As_xSe_{(100-x)}$, $0 \leq x \leq 40$) bulk glasses according to ref. 55. Our data on nanohardness (H_{ind}) were added to the graph after unit conversion for both As–S and As–Se bulk glasses (dashed line marked as "b" with star and circles, respectively) and As–S and As–Se thin films (dashed line marked as "tf", with star and circles, respectively). It also should be noted that we assumed T_g(film) ± 20 °C = T_g(bulk). In all cases, the lines are included as mere guides for the eye.

evident that this correlation satisfies the relation $T_g = K(H - B)$ suggested by Shkol'nikov.[56] Because for Se–As_2Se_3 glasses the relation between T_g and the average coordination number (<r>) is linear, see e.g. the work of Boolchand et al.,[57] it is not surprising that the relation between H_v values for Se–As_2Se_3 glasses and T_g, <r>, inclusive of our H_{ind} values, should also be linear as found by Hach et al.[58]

Table 4 also shows the nanohardness (H_{ind}) of all prepared thin films evaporated onto the glass substrate and it could be seen that their nanohardness is lower in all cases than that of the corresponding bulk glasses. The nanohardness varied from 2.01 to 1.88 GPa for As_2S_3 and As_2Se_3 thin films evaporated onto the glass substrate, respectively. Furthermore, the same trend as for the bulk glasses was found, thus the nanohardness of As_1Se_{99} thin film evaporated onto the glass substrate (H_{ind} = 1.08 GPa) was much lower in comparison with As_2S_3 and As_2Se_3 thin films evaporated onto the same substrate (Table 4). The nanohardness (H_{ind}) of the thin films was lower in comparison with bulk glasses in the range between 0.21–0.43 GPa depending on the chemical composition. The decrease of the thin films nanohardness in comparison with the corresponding bulk glass equals ≈ 21 rel% and 19 rel% for As_2S_3 and As_1Se_{99} glasses, and ≈ 17 rel% for As_2Se_3 glass. The comparable trend was also published by Shchurova et al.[59] and they showed in their work that the mechanical properties like Young's modulus or microhardness of As_2S_3 and As_2Se_3 bulk glasses among others are higher in comparison with the corresponding thin films. The authors attributed these to the packing density, that is the ratio between the films and bulk glasses density. Table 4 also shows that the influence of different substrates (glass and Si)

used for the preparation of thin films was, with respect to the experimental, almost negligible and this is in harmony with the data published by Pelegri et al.[60] and Menčík et al.[61] These authors, however, did not study chalcogenide glasses.

The decrease in the thin film nanohardness in comparison with the corresponding bulk glasses is in harmony with our previously mentioned results in chapters 3.3 and 3.4, thus with a decrease of density and refractive index of the thin films with respect to their corresponding bulk glasses. The results for As_2S_3 and As_1Se_{99} materials are comparable, thus the decrease of refractive index and density of thin films in comparison with their corresponding bulk glasses was in the order of 1–2 rel%, while the decrease of nanohardness of thin films in comparison with their corresponding bulk glasses was ≈ 20 rel% (see Tables 1, 2 and 4).

Additionally, the difference not only between the refractive index and density of As_2S_3 bulk glass and corresponding thin film, but also between their structures, was observed. The structure depolymerization for the As_2S_3 virgin thin film was observed, which leads to the decrease in the thin film cohesion, and this in all probability also contributed to the highest decrease of nanohardness in comparison with the corresponding bulk glass. After the annealing of the As_2S_3 thin film which was accompanied with the structure polymerization, the structure became comparable to that of bulk glass and the nanohardness of As_2S_3 thin film increased to 2.08 GPa as shown in Table 4. This increase in the As_2S_3 thin film nanohardness, however, did not have much influence on the relative difference between the nanohardness of the As_2S_3 thin film and its corresponding bulk glass. Furthermore, although the highest relative difference between the As_2Se_3 thin film and corresponding bulk glass was found from the point of refractive index and density (see Table 1 and 2), that the nanohardness difference between the As_2Se_3 thin film and corresponding bulk glass was lower (17 rel%) in comparison with the As_2S_3 and As_1Se_{99} materials (≈ 20 rel%). However, this does not change the fact that the nanohardness of all thin films was lower than the corresponding bulk glasses, and the reason for such a difference in behavior of the As_2Se_3 materials in comparison with As_2S_3 and As_1Se_{99} samples will be the subject of further research.

4. Conclusion

Our results can be summarized as follows:

(i) Density, structure and nanohardness were compared for all the bulk glasses and corresponding thin films, whose density, using their accurate weighing, was determined.

(ii) A major part of the observed changes in the refractive index between virgin films and the corresponding bulk glasses was explained, using the Lorentz–Lorenz relation, mainly by lowering the thin films density in comparison with the density of the corresponding bulk glasses.

(iii) The Raman spectra showed a similar structural arrangement for both the As_2Se_3 and As_1Se_{99} bulk glasses and thin films and, as is well known, confirmed the different structural arrangement for the As_2S_3 bulk and virgin thin films.

At the same time, the differences in the density between As_2Se_3 and As_1Se_{99} bulk glasses and their corresponding thin films is much higher than the differences in the density of As_2S_3 and the corresponding thin films. This is explained by the role of empty volume in the case of the bulk glasses and As_2Se_3 and As_1Se_{99} thin films, and by depolymerization in the As_2S_3 thin film.

(iv) Last, but not the least, the nanohardness of all bulk glasses and corresponding thin films was also compared. The nanohardness of all thin films was in all cases lower than that of the corresponding bulk glasses. This result is in harmony with lower values of thin films density with the respect to their corresponding bulk glasses. Linear correlation between the nanohardness and the glass transition temperature was found.

Conflicts of interest

There are no conflicts to declare.

Acknowledgements

References

1 R. Zallen, *The Physics in Amorphous Solids*, Wiley-VCH Verlag GmbH & Co. KGaA, 2007.

2 J.-L. Adam and X. E. Zhang, *Chalcogenide Glasses Preparation, Properties and Applications*, Woodhead Publishing Ltd, 2013.

3 R. I. Alekberov, S. I. Mekhtiyeva, A. I. Isayev and M. Fabian, *J. Non-Cryst. Solids*, 2017, **470**, 152–159.

4 R. I. Alekberov, S. I. Mekhtiyeva, A. I. Isayev, M. Fabian, Q. Tian and L. Almasy, *Chalcogenide Lett.*, 2017, **14**, 79–85.

5 R. I. Alekberov, A. I. Isayev, S. I. Mekhtiyeva and M. Fabian, *Phys. B*, 2018, **550**, 367–375.

6 H. A. Lorentz, *Ann. Phys.*, 1880, **9**, 641–665.

7 L. Lorenz, *Ann. Phys.*, 1880, **11**, 70–103.

8 Y. Saito, S. Hatayama, Y. Shuang, S. Shindo, P. Fons, A. V. Kolobov, K. Kobayashi and Y. Sutou, *Appl. Phys. Express*, 2019, **12**, 051008.

9 M. Frumar, Z. Polak, M. Vlcek and Z. Cernosek, *J. Non-Cryst. Solids*, 1997, **221**, 27–33.

10 P. Němec, J. Jedelsky, M. Frumar, M. Stabl and M. Vlcek, *J. Phys. Chem. Solids*, 2004, **65**, 1253–1258.

11 M. Samuelsson, D. Lundin, J. Jensen, M. A. Raadu, J. T. Gudmundsson and U. Helmersson, *Surf. Coat. Technol.*, 2010, **205**, 591–596.

12 A. Waseda, K. Fujii and N. Taketoshi, *IEEE Trans. Instrum. Meas.*, 2005, **54**, 882–885.

13 P. Viščor and D. Allan, *Thin Solid Films*, 1979, **62**, 259–263.

14 M. Yasaka, *Rigaku J.*, 2010, **26**, 1–9.

15 B. Ilic, S. Krylov and H. Craighead, *Proc. IEEE*, 2009, 650–653.

16 W. E. Wallace, D. L. Jacobson, M. Arif and A. Ioffe, *Appl. Phys. Lett.*, 1999, **74**, 469–471.

17 H. F. Xiang, Z. X. Xu, V. A. L. Roy, C. M. Che and P. T. Lai, *Rev. Sci. Instrum.*, 2007, **78**, 034104.

18 R. Swanepoel, *J. Phys. E: Sci. Instrum.*, 1983, **16**, 1214–1222.

19 J. B. Pethica, R. Hutchings and W. C. Oliver, *Philos. Mag. A*, 1983, **48**, 593–606.

20 F. Spaepen and A. L. Shull, *Curr. Opin. Solid State Mater. Sci.*, 1996, **1**, 679–683.

21 J. P. Guin, T. Rouxel, J. C. Sangleboeuf, I. Melscoet and J. Lucas, *J. Am. Ceram. Soc.*, 2002, **85**, 1545–1552.

22 M. L. Trunov, S. N. Dub, P. M. Nagy and S. Kokenyesi, *J. Phys. Chem. Solids*, 2007, **68**, 1062–1068.

23 T. Sabapathy, M. Kiran, A. Ayiriveetil, A. K. Kar, U. Ramamurty and S. Asokan, *Opt. Mater. Express*, 2013, **3**, 684–690.

24 J. N. Ding, G. X. Xie, Z. Fan, Y. Z. Fu and Z. Y. Ling, *J. Wuhan Univ. Technol.*, 2007, **22**, 196–200.

25 T. M. Rajakumar, V. Uma and R. Chandramani, *Indian J. Pure Appl. Phys.*, 2013, **51**, 131–137.

26 A. G. Prabhudessai, S. Balaji, K. Biswas, R. Dasgupta, P. Sarkar and K. Annapurna, *J. Non-Cryst. Solids*, 2019, **507**, 56–65.

27 P. Kutalek, E. Cernoskova, L. Benes, P. Knotek, Z. Cernosek and L. Tichy, *J. Non-Cryst. Solids*, 2017, **478**, 75–78.

28 J. Tauc, *Amorphous and liquid semiconductors*, ed. J. Tauc, Plenum, New York, 1974.

29 R. Shuker and R. W. Gammon, *Phys. Rev. Lett.*, 1970, **25**, 222–225.

30 E. Márquez, J. M. GonzalezLeal, R. Jimenez Garay, S. R. Lukic and D. M. Petrovic, *J. Phys. D: Appl. Phys.*, 1997, **30**, 690–702.

31 J. M. S. Prewitt and M. L. Mendelsohn, *Ann. N. Y. Acad. Sci.*, 1966, **128**, 1035–1053.

32 P. K. Sahoo, S. Soltani and A. K. C. Wong, *Computer Vision, Graphics, and Image Processing*, 1988, vol. 41, pp. 233–260.

33 P. Knotek, M. Vlcek, M. Kincl and L. Tichy, *Thin Solid Films*, 2012, **520**, 5472–5478.

34 W. C. Oliver and G. M. Pharr, *J. Mater. Res.*, 2004, **19**, 3–20.

35 S. Tsuchihashi and Y. Kawamoto, *J. Non-Cryst. Solids*, 1971, **5**, 286–305.

36 T. Cardinal, K. A. Richardson, H. Shim, A. Schulte, R. Beatty, K. Le Foulgoc, C. Meneghini, J. F. Viens and A. Villeneuve, *J. Non-Cryst. Solids*, 1999, **256**, 353–360.

37 V. I. Mikla and V. V. Mikla, *J. Optoelectron. Adv. Mater.*, 2010, **12**, 1827–1839.

38 J. Holubova, Z. Cernosek and E. Cernoskova, *J. Non-Cryst. Solids*, 2009, **355**, 2050–2053.

39 R. Todorov, D. Tsankov, J. Pirov and K. Petkov, *J. Phys. D: Appl. Phys.*, 2011, **44**, 305401.

40 R. P. Wang, S. J. Madden, C. J. Zha, A. V. Rode and B. Luther-Davies, *J. Appl. Phys.*, 2006, **100**, 063524.

41 R. Golovchak, O. Shpotyuk, J. S. Mccloy, B. J. Riley, C. F. Windisch, S. K. Sundaram, A. Kovalskiy and H. Jain, *Philos. Mag.*, 2010, **90**, 4489–4501.

42 D. Y. Choi, S. Madden, A. Rode, R. P. Wang and B. Luther-Davies, *J. Appl. Phys.*, 2007, **102**, 083532.

43 V. I. Mikla and V. V. Mikla, *Optoelectron. Adv. Mater., Rapid Commun.*, 2007, **1**, 272–276.

44 P. Nemec, J. Jedelsky, M. Frumar, Z. Cernosek and M. Vlcek, *J. Non-Cryst. Solids*, 2005, **351**, 3497–3502.

45 M. L. Slade and R. Zallen, *Solid State Commun.*, 1979, **30**, 357–360.

46 D. Y. Choi, A. Wade, S. Madden, R. P. Wang, D. Bulla and B. Luther-Davies, *Phys. Procedia*, 2013, **48**, 196–205.

47 Z. Polak, M. Frumar and B. Frumarova, *Thin Solid Films*, 1999, **343**, 484–487.

48 G. Lucovsky, *Physics of Selenium and Tellurium*, Springer-Verlag Berlin, 1979.

49 Y. Ito, S. Kashida and K. Murase, *Solid State Commun.*, 1988, **65**, 449–452.

50 Harvard University, Department of Physics, 2007, http://ipl.physics.harvard.edu/wp-uploads/2013/03/PS3E.

51 J. P. De Neufville, S. C. Moss and S. R. Ovshinsky, *J. Non-Cryst. Solids*, 1974, **13**, 191–223.

52 D. J. Treacy, P. C. Taylor and P. B. Klein, *Solid State Commun.*, 1979, **32**, 423–427.

53 P. Bonazzi, S. Menchetti and G. Pratesi, *Am. Mineral.*, 1995, **80**, 400–403.

54 T. Kavetskyy, J. Borc, K. Sangwal and V. Tsmots, *J. Optoelectron. Adv. Mater.*, 2010, **12**, 2082–2091.

55 Z. U. Borisova, *Glassy Semiconductors*, Plenum Press, New York, 1981.

56 E. V. Shkol'nikov, *Sov. J. Glass Phys. Chem.*, 1985, **11**(1), 50–55.

57 P. Boolchand, D. G. Georgiev, T. Qu, F. Wang, L. Cai and S. Chakravarty, *C. R. Chim.*, 2002, **5**, 713–724.

58 C. T. Hach, K. CerquaRichardson, J. R. Varner and W. C. LaCourse, *J. Non-Cryst. Solids*, 1997, **209**, 159–165.

59 T. N. Shchurova and N. D. Savchenko, *J. Optoelectron. Adv. Mater.*, 2001, **3**, 491–498.

60 A. A. Pelegri and X. Huang, *Compos. Sci. Technol.*, 2008, **68**, 147–155.

61 J. Menčík, in *Emerging Nanotechnologies in Dentistry (Second Edition), Micro and Nano Technologies*, William Andrew Applied Science Publishers, 2018.

62 J. Holubova, Z. Cernosek and E. Cernoskova, *J. Optoelectron. Adv. Mater.*, 2007, **9**, 1979–1984.

63 L. Tichý, H. Tichá, P. Nagels, R. Callaerts, R. Mertens and M. Vlcek, *Mater. Lett.*, 1999, **39**, 122–128.